

SIMULATION OF EXTREME WAVE INTERACTION WITH MONOPILE MOUNTS FOR OFFSHORE WIND TURBINES

Feng Gao¹, Clive Mingham¹ and Derek Causon¹

Extreme wave run-up and impacts on monopile foundations may cause unexpected damage to offshore wind farm facilities and platforms. To assess the forces due to wave run-up, the distribution of run-up around the pile and the maximum wave run-up height need to be known. This paper describes a numerical model AMAZON-3D study of wave run-up and wave forces on offshore wind turbine monopile foundations, including both regular and irregular waves. Numerical results of wave force for regular waves are in good agreement with experimental measurement and theoretical results, while the maximum run-up height are little higher than predicted by linear theory and some empirical formula. Some results for irregular wave simulation are also presented.

Keywords: extreme wave; monopile; numerical simulation; wave run-up; wave force

INTRODUCTION

During the last decade, a large number of offshore wind farms were built. Observations on existing wind farms have clearly shown that wave interaction with monopile foundations can be quite significant (De Vos et al. 2007). Wave run-up and wave impacts may cause unexpected damage to wind farm facilities and platforms. To assess the forces due to wave run-up, the distribution of run-up around the pile and the maximum run-up height need to be known.

Previously, run-up on circular cylinders has been studied experimentally and mathematically. By using linear wave diffraction theory, Sarpkaya and Isaacson (1981) obtained results for the wave elevation around a circular cylinder surface. Niedzwecki and Duggal (1992) performed a small-scale experimental study to investigate wave run-up on rigid full length and truncated circular cylinders under regular and random wave conditions. They found that linear diffraction theory underestimates the wave run-up for all but very low wave steepness and employed a semi-empirical variation of the formula to predict the wave run up. Chan et al. (1995) studied the run-up and especially the forces on a circular cylinder under the influence of a plunging breaker. From that study it became clear that the breaking process has a great impact on the maximum horizontal forces and also influences the run-up. Kriebel (1998) focused on the run-up for periodic waves on a plane bed. The results were compared with 1st and 2nd order analytical wave diffraction theories and indicated that the non-linearity of the waves has a large effect on the total run-up. Büchmann et al. (1998) used a second order boundary integral method to study run-up on a structure with and without an ambient current. Mase et al. (2001) set up analytical equations for the run-up on small diameter foundations without explicitly including the diameter of the cylinder, even though basic diffraction theories appear to show that the diameter has a clear effect on the run-up. Martin et al. (2001) investigated run-up on columns caused by steep regular waves in deep water. They compared their experimental results with various theories and conclude that most theories underestimate the run-up values and the semi-empirical method suggested by Niedzwecki and Huston (1992) overestimated the run up in most of the test cases considered. Recently, De Vos et al. (2007) suggested a new formula for prediction of the maximum wave run-up on monopile foundation, which is based on a small-scale experimental study that examines both regular and irregular wave run-up on cylindrical pile foundations.

In this paper, some results of numerical simulations involving regular and extreme wave impact and run-up on monopile foundations for offshore wind turbines will be presented. Simulations were carried out by using the AMAZON-3D code, which solves the incompressible Navier-Stokes equations in both air and water regions simultaneously with the free surface captured automatically as a contact surface in the density field. A time-accurate artificial compressibility method and high Godunov-type scheme was adopted to replace the pressure correction solver used in other methods (Qian et al. 2006). The Cartesian cut cell technique was used to generate a boundary fitted mesh. The advantages of this approach were outlined by Causon et al. (2001) including its flexibility for dealing with arbitrarily complex geometries and moving bodies.

¹ Centre for Mathematical Modelling and Flow Analysis, School of Computing, Mathematics & Digital Technology, Manchester Metropolitan University, Chester Street, Manchester, M1 5GD, United Kingdom

NUMERICAL METHOD

Governing equations and numerical solution

For incompressible, unsteady, viscous flows, the Navier-Stokes equations with a variable density field can be modified using the artificial compressibility method and written in the integral form:

$$\frac{\partial}{\partial t} \iiint_{\Omega} Q \delta\Omega + \oint_S (F_c - F_v) \delta S = \iiint_{\Omega} B \delta\Omega \quad (1)$$

in which Q represents the vector of flow variables, F_c and F_v are the convective and viscous flux terms, and B stands for the source terms. They are defined as follows:

$$Q = \begin{bmatrix} \rho \\ \rho u \\ \rho v \\ \rho w \\ p/\beta \end{bmatrix}, \quad F_c = \begin{bmatrix} \rho U \\ \rho u U + n_x p \\ \rho v U + n_y p \\ \rho w U + n_z p \\ U \end{bmatrix}, \quad F_v = \begin{bmatrix} 0 \\ n_x \tau_{xx} + n_y \tau_{xy} + n_z \tau_{xz} \\ n_x \tau_{yx} + n_y \tau_{yy} + n_z \tau_{yz} \\ n_x \tau_{zx} + n_y \tau_{zy} + n_z \tau_{zz} \\ 0 \end{bmatrix}, \quad B = \begin{bmatrix} 0 \\ 0 \\ -\rho g \\ 0 \\ 0 \end{bmatrix} \quad (2)$$

where ρ is the density, p is the pressure, β is the compressibility coefficient, g is the gravitational acceleration. $U = u \cdot n_x + v \cdot n_y + w \cdot n_z$ is the contra-variant velocity and $\mathbf{n} = (n_x, n_y, n_z)$ is the outward pointing unit normal vector at a mesh cell face.

The viscous stress tensor is defined as $\tau_{ij} = 2\mu S_{ij}$, in which μ is the dynamic viscosity and S_{ij} is the rate of the strain tensor defined as

$$S_{ij} = \frac{1}{2} \left(\frac{\partial u_i}{\partial x_j} + \frac{\partial u_j}{\partial x_i} \right) \quad (3)$$

The flow equations (1) are discretised by the cell-centred finite volume method over each cell of the flow domain, which gives

$$\frac{\partial Q_{ij} \Omega_{ij}}{\partial t} = - \oint_{\partial\Omega_{ij}} (F_c - F_v) dS + B_{ij} \Omega_{ij} = -R(Q_{ij}) \quad (4)$$

where Ω_{ij} indicates the grid cell indexed by the subscript ij and R is the residual of the flow equations. Supposing the grid cell Ω_{ij} has m faces then integration of the fluxes across the faces will result in

$$\sum_{k=1}^m (F_c - F_v)_k \Delta l_k = \int_{k=1}^m (F_c - F_v)_k \Delta l_k \quad (5)$$

The convective flux across a grid cell face is computed by Roe's approximate Riemann solver

$$F_{c,k} = \frac{1}{2} \left[F_c(Q_k^+) + F_c(Q_k^-) - |A| (Q_k^+ - Q_k^-) \right] \quad (6)$$

where Q_k^+ and Q_k^- are the reconstructed data values on the right and left of face k , A is the Jacobian matrix which can be expressed as

$$A = \begin{bmatrix} 0 & n_x & n_y & n_z & 0 \\ -uU & un_x + U & un_y & un_z & \beta n_x \\ -vU & vn_x & vn_y + U & vn_z & \beta n_y \\ -wU & wn_x & wn_y & wn_z + U & \beta n_z \\ -U/\rho & n_x/\rho & n_y/\rho & n_z/\rho & 0 \end{bmatrix} \quad (7)$$

The eigenvalues of the matrix are

$$\lambda_{1,2,3} = U, \quad \lambda_{4,5} = \frac{1}{2}(U \pm c), \quad c = \sqrt{U^2 + 4\beta/\rho} \quad (8)$$

More details of the finite volume solution method for incompressible two-fluid flows on a Cartesian cut cell mesh can be found in the work of Qian et al. (2006) and Gao et al. (2007).

By discretizing equation (4) in time and omitting the subscripts for simplicity, the following first-order Euler implicit difference scheme can be employed

$$\frac{(Q\Omega)^{n+1} - (Q\Omega)^n}{\Delta t} = -R(Q^{n+1}) \quad (9)$$

To achieve a time-accurate solution at each physical time step in unsteady flow problems, equation (9) must be further modified to obtain a divergence free velocity field. This is accomplished by introducing a pseudo time derivative into the system of equations, as

$$\frac{(Q\Omega)^{n+1,m+1} - (Q\Omega)^{n+1,m}}{\Delta \tau} + I_{ta} \frac{(Q\Omega)^{n+1,m+1} - (Q\Omega)^{n,m}}{\Delta t} = -R(Q^{n+1,m+1}) \quad (10)$$

where τ is the pseudo time and $I_{ta} = \text{diag}[1, 1, 1, 1, 0]$. The right hand side of equation (10) can be linearized using Newton's method at the $m + 1$ pseudo-time level to yield

$$\left[I_m \Omega + \frac{\partial R(Q^{n+1,m})}{\partial Q} \right] (Q^{n+1,m+1} - Q^{n+1,m}) = - \left[I_{ta} \frac{(Q^{n+1,m+1} - Q^{n,m})}{\Delta t} \Omega + R(Q^{n+1,m}) \right] \quad (11)$$

where $I_m = \text{diag}[1/\Delta\tau + 1/\Delta t, 1/\Delta\tau + 1/\Delta t, 1/\Delta\tau + 1/\Delta t, 1/\Delta\tau + 1/\Delta t, 1/\Delta\tau]$. When $\Delta(Q^{n+1})^m = Q^{n+1,m+1} - Q^{n+1,m}$ is iterated to zero at each time step, the density and momentum equations are satisfied identically and the divergence of the velocity at time level $n + 1$ is zero. The system of equations can be written in matrix form as

$$(D + L + U)\Delta Q^s = RHS \quad (12)$$

where D is a block diagonal matrix, L is block lower triangular matrix, and U is a block upper triangular matrix. Each of the elements in these matrices is a 5×5 matrix. An approximate LU factorization (ALU) scheme can be adopted to obtain the inverse of equation (12) in the form

$$(D + L)D^{-1}(D + U)\Delta Q^s = RHS \quad (13)$$

Within each time step of the implicit integration process, the sub-iterations are terminated when the L_2 norm of the change in successive sub-iterations

$$L_2 = \left\{ \left[\sum_1^N (Q^{s+1} - Q^s)^2 \right] / N \right\}^{1/2} \quad (14)$$

is less than a specified limit ϵ . In the present study this value is set $\epsilon = 10^{-4}$.

Wave generation

In the numerical wave tank, the three components of velocity are specified at the inflow boundary to generate the required wave with the pressure and density extrapolated from the interior of the computational domain by assuming zero spatial gradients. This definition allows the desired waves to propagate into the computational domain through this boundary.

For regular wave generation, linear wave theory is used to calculate the input velocity profile and wave elevation; however, for an extreme wave, the exact velocity profile for a true physically realisable nonlinear wave under the given conditions is not known a priori. Thus, a viable approach is to input reasonable approximate wave conditions along the inflow boundary to simulate the real phenomenon. This leads to the notion of the extreme wave formulation as a focused wave group in which many wave components in a spectrum are focussed simultaneously at a particular position in space in order to model the average shape of an extreme wave profile consistent with the random process within a specified wave energy spectrum. The derivation here refers to the works of Dalzell (1999) and Ning et al. (2009) in which a first or second-order Stokes focused wave can be imposed in such a manner.

Assuming waves are focused at a specified point x_f at time t_f , linear wave theory defines the wave elevation at an arbitrary point as

$$\eta(x, t) = \sum_{i=1}^N a_i \cos[k_i(x - x_f) - 2\pi f_i(t - t_f)] \quad (15)$$

where N is the total number of wave components, and a_i , k_i , f_i represent the wave amplitude, the wave number and the wave frequency of the i th wave component, respectively. The dispersion relation establishes the relation between space and time, i.e. between k_i and f_i .

With a chosen wave energy frequency spectrum and by setting the phases of all the wave components as zero at the focal point, the amplitude a_i of each wave component i can be calculated from

$$a_i = A_F \frac{S_i(f)\Delta f}{\sum_{i=1}^N S_i(f)\Delta f} \quad (16)$$

where $S_i(f)$ is the desired frequency spectrum, Δf is the increment in frequency depending on the number of wave components and the frequency band width and A_F is the total input wave amplitude of the focused wave.

In this study, a JONSWAP wave spectrum formulated as (17) is selected to generate the extreme wave. Where $H_{\frac{1}{3}}$ is the significant wave height; T_p and f_p are the peak wave period and frequency respectively. The peak enhancement factor γ_a is chosen as 3.3.

$$S(f) = \beta_J H_{\frac{1}{3}}^2 T_p^{-4} f^{-5} \exp[-1.25(T_p f)^{-4}] \gamma_a^{\exp[-(T_p f - 1)^2 / 2\lambda^2]} \quad (17)$$

$$\beta_J \cong \frac{0.06238(1.094 - 0.01915 \ln \gamma_a)}{0.230 + 0.0336\gamma_a - 0.185(1.9 + \gamma_a)^{-1}} \quad (18)$$

$$\lambda = \begin{cases} 0.07 & f \leq f_p \\ 0.09 & f > f_p \end{cases} \quad (19)$$

Force calculation

The analytical solution of the linearized diffraction problem for a circular cylinder at arbitrary water depths was given by MacCamy and Fuchs (1954). Accordingly, the first-order non-dimensional maximum horizontal force \bar{F}_{\max} is

$$\bar{F}_{\max} = \frac{F_{\max}}{\rho g h H r (\tanh kh / kh)} = 2 \frac{[J_1^2(kr) + Y_1^2(kr)]^{-1/2}}{kr} \quad (20)$$

where ρ is the water density, h is the water depth, k is the wave number, H is the incident wave height, r is the cylinder radius, and $J_1(kr)$ and $Y_1(kr)$ are derivatives of the Bessel functions of the first and second kind of order one respectively.

For a vertical circular cylinder in finite water depth, Kriebel (1990) presented a complete closed-form solution for the velocity potential resulting from the interaction of second-order plane waves; Rahman et al. (1999) also presented an analytical solution for the second order wave force.

In this numerical simulation, the pressure p can be obtained from the derived p/β by solving the governing equations (1). The total force is obtained by integration of the pressure field around the cylinder contour

$$F = - \int_{S_b} p n dS \quad (21)$$

where S_b is the cylinder surface as defined approximately by the boundary fitted cut cell surface.

Wave run-up

Using different approaches Kriebel (1992) and Martin et al. (2001) have carried out an extension of diffraction theory to the second order. They found that there is a large influence of using second order theory to calculate run-up and it is not sufficient to attempt an extrapolation based on linear diffraction theory. However, they have given the following approximate result for run-up on the up-wave side of a circular cylinder

$$\frac{R_u}{\eta_{\max}} = \left[1 + \left(\frac{2\pi D}{L} \right)^2 \right]^{1/2} \quad (22)$$

where R_u is the predicted wave run-up, D is the diameter of cylinder, L is the wave length and η_{\max} is the wave crest.

The threshold of linear diffraction is widely regarded as $D/L < 0.2$. In this range, linear diffraction theory suggests that the scattered wave energy is negligibly small. However, this is not the case for steep waves. There are significant nonlinear contributions in the case of steep waves; thus, fully nonlinear modeling is advisable for a steep wave run-up calculation.

Recently, De Vos et al. (2007) suggested a new formula to predict the maximum wave run-up on a cylindrical foundation based on a small-scale experimental study as follows

$$R_{u \max} = 1.22 \left(\eta_{\max} + 2.71 \frac{u^2}{2g} \right) \quad (23)$$

where η_{\max} is the maximum wave elevation and u is the horizontal particle velocity at the wave crest.

$$\eta_{\max} = \frac{H}{2} + k \frac{H}{2} \frac{H \cosh(kd)}{8 \sinh^3(kd)} (2 + \cosh(2kd)) \quad (24)$$

$$u = \frac{H}{2} \frac{gk}{\omega} \frac{\cosh(k(\eta_{\max} + d))}{\cosh(kd)} + \frac{3}{4} k \frac{H^2}{4} \frac{\omega \cosh(2k(\eta_{\max} + d))}{\sinh^4(kd)} \quad (25)$$

where H is the incident wave height, g is the gravitational acceleration, d is the still water depth, k is the wave number and ω is the wave frequency.

NUMERICAL RESULTS

The present numerical simulations were first carried out with regular waves and then with extreme waves. The numerical wave tank has dimensions $8\text{m} \times 3.6\text{m} \times 0.9\text{m}$, with a still water depth of 0.45m (Fig. 1). A circular cylinder of diameter 0.325m is positioned with its center at the middle of the tank. Different waves are generated at the left inflow boundary with propagation to the right. The right side boundary is set as open boundary which allows fluids to freely enter or leave the computational domain according to the local flow velocity and direction. The front and back side wall boundaries are set as solid walls. Several wave gauges are set along the center line of the tank to record wave elevations.

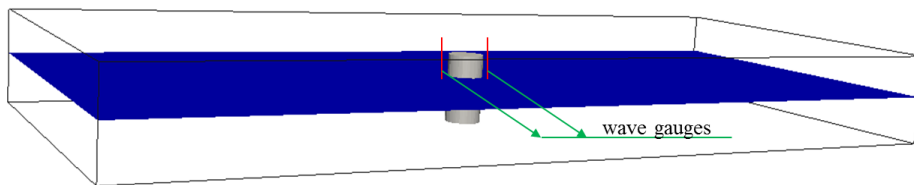


Figure 1. Numerical wave tank set up

A non-uniform block structure mesh was used in the background of the computation domain; a relatively fine mesh was used in the area near the cylinder and around the water free surface. Around the structure of cylinder, the Cartesian cut cell technique was used to generate a fully boundary-fitted mesh. Details of the Cartesian cut cell technique can be found in the works of Causon et al. (2001) and Ingram et al. (2003). Part of the 3D computational mesh around the vertical circular cylinder is shown in Fig. 2. Totally there are $258 \times 39 \times 62$ cells in the domain with the size of smallest cell of dimension 0.02m .

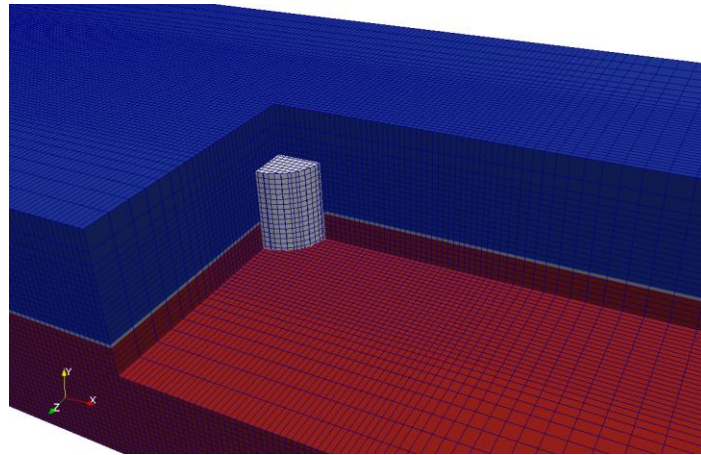
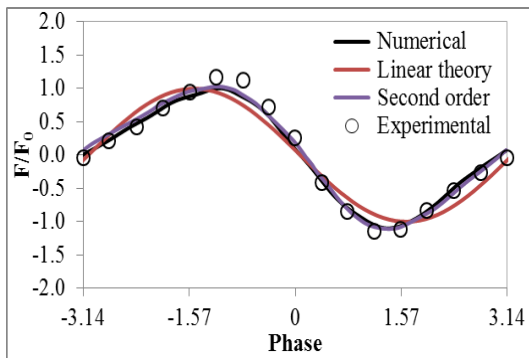


Figure 2. 3D computational mesh around the vertical cylinder (blue parts are in air and red parts are in water)

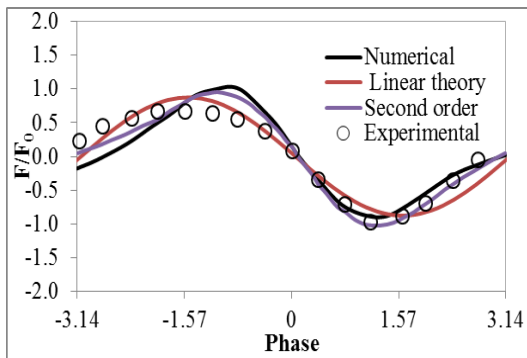
Regular wave simulation

Four simulations are carried out for regular waves and compared with theoretical and experimental data found in Kriebel(1998). The parameters of these test cases are shown in Table 1, where A_m is wave amplitude, T is wave period and kr is the scattering parameter corresponding to wave number k and cylinder radius r .

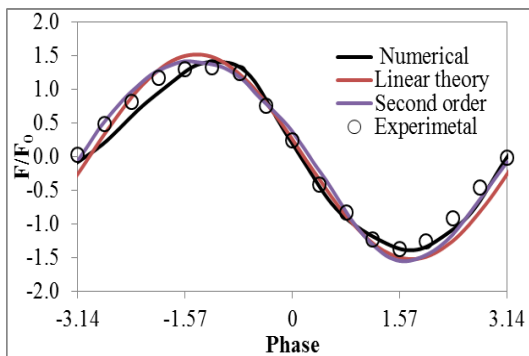
	Case1	Case2	Case3	Case4
A_m (m)	0.0535	0.048	0.0621	0.074
T (s)	1.95	1.75	1.50	1.25
kr	0.271	0.308	0.374	0.481



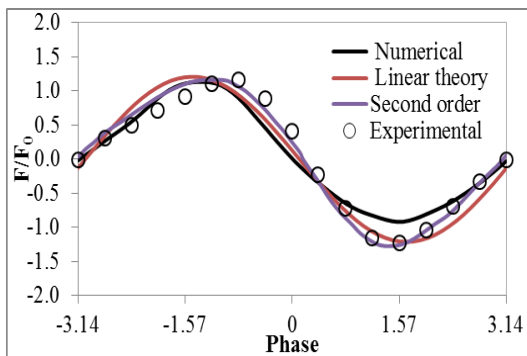
(a) case1: $kr = 0.271$, $kH = 0.178$



(b) case2: $kr = 0.308$, $kH = 0.182$



(c) case3: $kr = 0.374$, $kH = 0.286$



(d) case4: $kr = 0.481$, $kH = 0.438$

Figure 3. Comparison of wave force time series for various combinations of kr and kH

Sample time series of horizontal force on the cylinder compared to measurements from Kriebel (1998) and both linear and second order analytical predictions are presented in Fig 3. Each figure shows the results over one wave period in which the wave crest phase is centered in the figure. It can be seen that numerical results are in generally good agreement with the experimental and theoretical results.

The numerical results for maximum wave run up compared with the approximation formulae are shown in Fig. 4. Although the present numerical results are a little higher than the empirical Eq. (23) predictions, they are acceptable, while Eq. (22) which is based on liner diffraction theory is much less accurate as Martin et al. (2001) has mentioned. Fig.5 shows the time history of wave elevation at different wave gauges for first two test cases. The locations of the wave gauges are along the center line of the wave tank; gauge 1 is located just in front of the cylinder and gauge 2 is just behind the cylinder. The wave run up situation can be seen clearly.

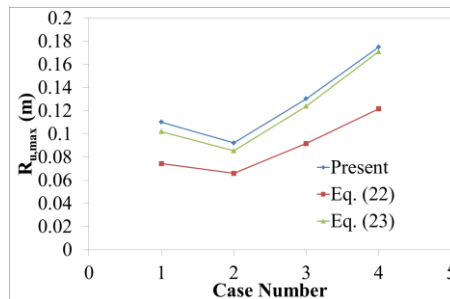


Figure 4. Comparison of maximum wave run-up

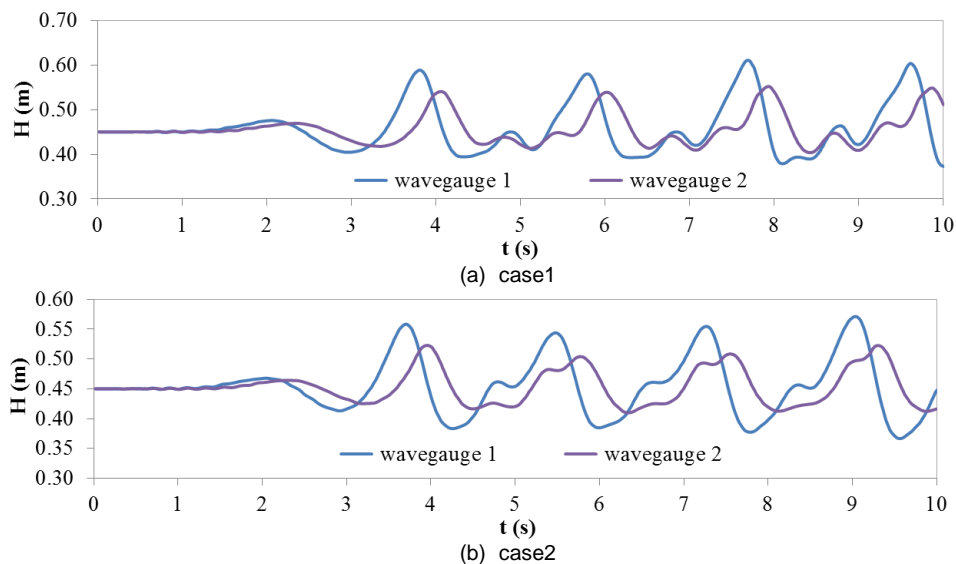


Figure 5. Time history of wave elevation at two different wave gauges for various cases

Extreme wave simulation

The calculation domain for the extreme wave simulations are almost the same as for the regular wave simulations, the only difference being that the center of the cylinder is moved to $x = 3.78\text{m}$. The focus point for the extreme wave is set just in front of the cylinder at $x = 3.61\text{m}$ and focus time is about 5.2s. Following the work of Ning et al. (2009), two test cases are chosen from their different experimental cases for these numerical simulations. The input characteristics of the relevant wave groups are listed in Table 2. The JONSWAP energy spectra with the same peak frequency $f_p = 0.83\text{Hz}$ is used.

Table 2. Input characteristics of wave groups for extreme wave				
Case	Frequency band f (Hz)	Input amplitude A_f (m)	Wave period T (s)	Wave length λ (m)
2	0.6-1.3	0.0632	1.20	2.00
3	0.6-1.4	0.0875	1.25	2.18

The time history of the horizontal forces acting on the cylinder for the two test cases is presented in Fig. 6. It can be seen that the maximum force appears around the focus time and larger amplitude waves produce larger impact forces. The maximum force is about 81.6N for case2 and 100.2N for case3, which are quite similar to the experiment results.

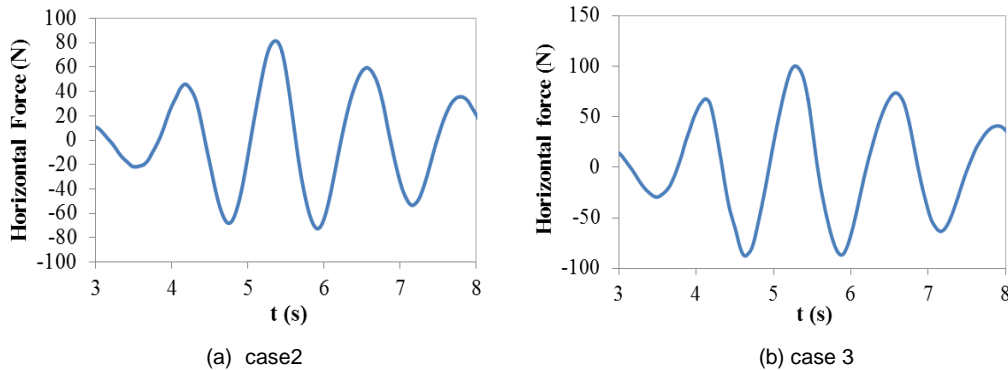


Figure 6. Time history of horizontal force acting on cylinder for various cases

Fig. 7 shows the time history of wave elevation at different wave gauges for these test cases. The location of the wave gauges is along the center line of wave tank with the one in front of the cylinder set at $x = 3.61\text{m}$ and the other just after the cylinder at $x = 3.95\text{m}$. The wave run-up can be seen clearly, and the maximum run-up appears close to the focus time. The value of maximum run-up height is about 0.110m for case2 and 0.152m for case3, which are a little higher than the predictions by empirical formula (23) as in the regular wave simulations.

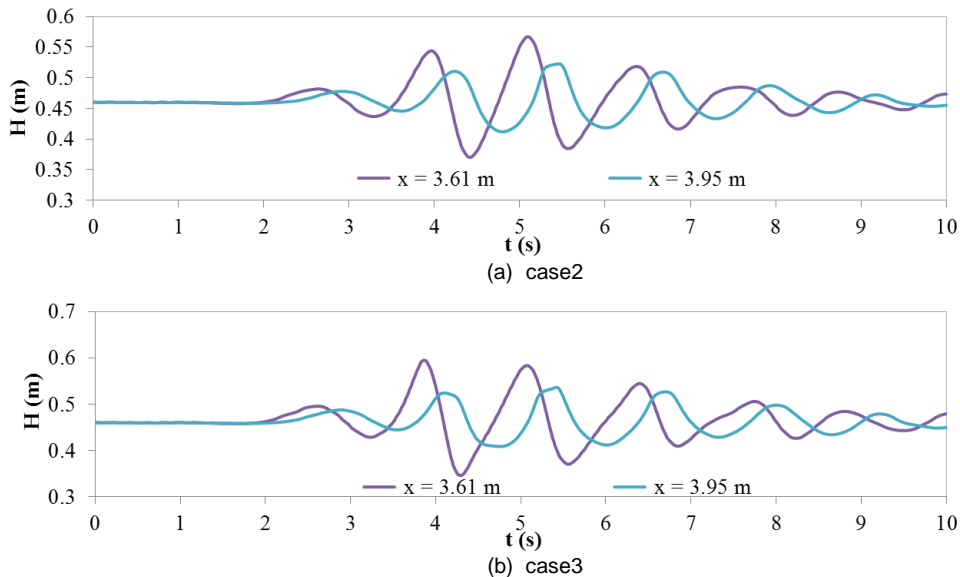


Figure 7. Time history of wave elevation at different wave gauges for various cases

CONCLUSIONS

The characteristics of wave run-up and horizontal wave force on the monopile foundation of an offshore wind turbine have been investigated numerically using a Navier-Stokes solver. The numerical results for wave force have been shown to be in good agreement with experiment measurements and results using second order theory. The maximum run-up height is only a little higher than the theoretical and empirical formulae predictions.

It can be concluded that the present flow code AMAZON-3D has the potential to be a usable tool for the detailed investigation of wave interactions with structures of this type. As the code can simulate breaking waves, further simulations including impacts from extreme waves breaking on offshore monopile mounts could be performed. In addition wave interactions with multiple structures will also be performed in the future.

ACKNOWLEDGMENTS

This work was financially supported by the EPSRC (UK), **Supergen Wind Energy Technologies Core, Towards the Offshore Wind Power Station**, under grant Ref: EP/H018662/1.

REFERENCES

- Büchmann, B., Skourup, J. and Cheung, K.F. 1998. Run-up on a structure due to second order waves and a current in a numerical wave tank, *Applied Ocean Research*, 20, 297-308.
- Causon D.M., Ingram D.M. and Mingham C.G. 2001. A Cartesian cut cell method for shallow water flows with moving boundaries. *Advances in Water resources*, 24, 899-911.
- Chan, E.S., Cheong, H.F. and Tan, B.C. 1995. Laboratory study of plunging wave impacts on vertical cylinders, *Coastal Engineering*, 25, 87-107.
- Dalzell J.F. 1999. A note on finite depth second-order wave-wave interactions. *Applied Ocean Research*, 21, 105–111.
- De Vos L., Frigaard P and De Rouck J. 2007. Wave run-up on cylindrical and cone shaped foundations for offshore wind turbines. *Coastal Engineering*. 54, 17–29.
- Gao F., Ingram D.M., Causon D.M. and Mingham C.G. 2007. The development of a Cartesian cut cell method for incompressible viscous flows, *International Journal for Numerical Methods in Fluids*, 54, 1033-1053.
- Ingram D.M., Causon D.M. and Mingham C.G. 2003. Developments in Cartesian cut cell methods. *Mathematics and Computers in Simulation*, 61, 561–572.
- Kriebel, D.L. 1990. Nonlinear wave diffraction by vertical circular cylinder. Part I: diffraction theory. *Ocean Engineering*, 17, 345–377.
- Kriebel, D.L. 1992. Nonlinear wave interaction with a vertical circular cylinder. Part II: Wave run-up, *Ocean Engineering*, 19, 75-99.
- Kriebel, D.L. 1998. Nonlinear wave interaction with a vertical circular cylinder: Wave Forces, *Ocean Engineering*, 25, 597-605.
- MacCamy, R.C. and Fuchs, R.A. 1954. Wave forces on piles: A diffraction theory. Technical memorandum no. 69. Beach Erosion Board Office of the Chief Engineers. Department of the Army. 1–17.
- Martin, A.J., Easson, W.J. and Bruce, T. 2001. Run-up on columns in steep, deep water regular waves. *Journal of Waterway, Port, Coastal, and Ocean Engineering* 127, 26–32.
- Mase, H., Kosho, K. and Nagahashi, S. 2001. Wave run-up of random waves on a small circular pier on sloping seabed. *Journal of Waterway, Port, Coastal and Ocean Engineering*. 127, 192–199.
- Niedzwecki, J.M. and Duggal, S.D. 1992. Wave run-up and forces on cylinders in regular and random waves. *Journal of Waterway, Port, Coastal, and Ocean Engineering*. 118, 615–634.
- Niedzwecki, J.M. and Huston, J.R. 1992. Wave interaction with tension leg platforms. *Ocean Engineering*. 19, 21–37.
- Ning D.Z., Zang J., Liu S.X., Eatock Taylor R. Teng B. and Taylor P.H., 2009. Free-surface and wave kinematics for nonlinear focused wave groups, *Ocean Engineering*. 36, 1226-1243.
- Qian L., Causon D.M., Mingham C.G. and Ingram D.M. 2006. A free-surface capturing method for two fluid flows with moving bodies, *Proceedings of the Royal Society London A*. 462, 21-42.
- Rahman, M., BORA, S.N. and Satish, M.G. 1999. A Note on Second-Order Wave Forces on a Circular Cylinder in Finite Water Depth. *Applied Mathematics Letters*, 12, 63-70
- Sarpkaya, T., Isaacson, M. 1981. *Mechanics of Wave Forces on Offshore Structures*. Van Nostrand Reinhold Co., New York.